Formation of TiO2/natural Melanin Nanostructure Hybrids with Enhanced Optical and Thermal Properties

nawal Madkhali (namadkhali@imamu.edu.sa)
Imam Muhammad Ibn Saud Islamic University https://orcid.org/0000-0002-7864-2578
Saja Algessair
Imam Muhammad bin Saud Islamic University: Imam Muhammad Ibn Saud Islamic University

Research Article

Keywords: Natural Melanin/TiO2, thermal stability, optoelectronic, Nanostructure, UV radiation

Posted Date: September 14th, 2021

DOI: https://doi.org/10.21203/rs.3.rs-632614/v1

Abstract

Recently, with the progress of research in amending and developing the properties of inorganic materials, researchers have become focused on using inexpensive and environmentally friendly materials such as organic materials from natural sources that have proven effective in improving the properties of materials in various applications. In recent years, melanin has become an attractive topic for researchers due to its distinctive structural properties that have been distinguished in various application fields. Here, we report the use of ultrasonication under UV radiation for synthesis. The influence of natural melanin on the structural, optical and thermal properties of TiO_2 nanoparticles was investigated by using Fourier transform infrared (FTIR) spectroscopy, thermogravimetric analysis (TGA) and UV–Vis spectroscopy. It was observed that incorporating natural melanin on TiO_2 nanoparticles (TiO_2-Mel) occurred at approximately 2.01 eV with low value of Urbach energy around 100 meV indicates improvement in crystalline structure. Thermal results showed that TiO_2-Mel is stable even with temperatures up to 400°C. According to the results obtained by the thermal stability of melanin with titanium dioxide can makes it a good candidate in many application such as solar cells and optoelectronic that require optical efficiency and thermal stability for long periods.

1. Introduction

One of the research areas that has attracted scientists in recent years is improving the properties of inorganic polymers in electronic, magnetic and optical applications. Organic-inorganic hybrids have received much research attention[1]. Many physicists and chemists researchers have been working to improve the properties of low-cost polymers and environmentally friendly to be used as an alternative to conventional semiconductor.

Titanium dioxide (TiO_2) is a kind of one of non-organic semiconductor in several applications and has unique advantages, for optical and photocatalytic applications[2, 3]. nontoxicity[4],and low cost[5]. Moreover, it can be prepared in various phases, such as thin film[6] pellet[7], or solution phases[8], by several techniques, such as pulsed laser deposition[9], sputtering[10] and chemical vapor deposition[11]. The thin film form is more suitable for photocatalysis because it enables the reuse of the photocatalyst without the need to separate it from the surrounding medium. In addition, oil slicks or spills can be treated easily by using thin films. Titanium dioxide has three polymorphs: anatase, rutile and brookite[12].

In the continuous search for organic–nonorganic hybrid, TiO_2 is one of the most investigated semiconductors. This is due to its distinctive: nontoxic, inexpensive, and photostable material [13]. Moreover, TiO_2 is individual electrochemical and optoelectrical attributes such as a high dielectric permittivity (around 64 at 1MHz frequency) [14] ,very high refractive index and excellent optical transmittance in the visible and IR regions and ,this has led to its common use in thin-film optics. Otherwise, it has a great photocatalytic in industrial applications[3]. Despite these advantages, titanium dioxide has a rather complex chemistry, so we find little research into grafting it with surface of organic polymers. More recently, literature has emerged that reports findings about the importance of titanium

dioxide with different polymers in water separation applications[15]. A recent study, reported the preparation and characterization of a polymer nanocomposite composed of TiO_2 in a polypyrrole matrix. The resulted composite might exhibit improved optomechanical properties. [16].

Hybrid nanoscale of organic and non-organic compounds can be synthesized a variety of different ways, providing many diverse characteristics of known compounds or can be synthesized as needed in specific applications.[17]. The nature of organic semiconductor materials is related to the presence of carbon, with hybridization between the s and p orbitals to form three sp2 orbitals with σ-bond. The fourth orbital, pz, is perpendicular to the plane of atoms, which produces an overlapped electronic component, namely, the π-bond[18]. This overlap is related to the mechanism of the electrical conductivity of the material. This is a relatively recent studies, focused on the modulation of the surface chemistry of non-organic nano-composite to improve their functional properties such as extending light absorption spectra[19].

Notably, melanin an organic conductor polymer, possesses unique properties. The oxidation products of 3,4-dihydroxyphenylalanine (DOPA), 5,6-dihydroxyindole (DHI) and 5,6-dihydroxyindloe-2-carboxylic acid (DHICA) are known as the main intermediates of melanin[20].However, synthetic melanin has very similar characteristics to natural melanin from herbal source such as Nigella Sativa. Recent studies have demonstrated that the content of DHICA-derived units in synthetic melanin is approximately 40% less than that of natural melanin[21]. Natural melanin is synthesized in vivo through a free radical-mediated process from its precursor, dopaquinone, which is generated by tyrosine, which in turn is produced through a tyrosinase-mediated process[22]. Melanin has a relatively diverse and heterogeneous structure. This is due to the ubiquitous sources of melanin, which leads to its heterogeneity in composition, size, color, and function[23]. It is considered one of the promising polymers due to its chemical properties that contain different functional groups. In recent years, melanin has shown stimulating results, especially in optical applications due to its high and wide optical absorption in the ultraviolet and visible region[24]. It can be considered as a class of soft conductor used in numerous technological applications including: memory devices[25], light emitting diodes and field effect transistors[26]

In this study, the thermostability and UV protective properties of natural melanin as organic materials and TiO_2 as inorganic nanocomposites were thoroughly investigated. This article has increased in importance in light of recent studies on the synthesis of natural eumelanin and TiO_2 nanocomposites while maintaining them original structures with high-temperature effects in thermal measurements. Moreover, and equally important, the study of the energy gap change in photometric measurements shows the possibility of using hybrid melanin and titanium dioxide in bioelectronic applications on a wider range than conventional semiconductors.

2. Experimental

2.1 Preparation

Anatase TiO_2 nanoparticles were purchased from Guangzhou Hongwu Material Technology Co., Ltd. The natural melanin powder used in this work was extracted from *Nigella sativa* (black seeds) using the same method reported in [24].The black seed coats were solubilized in a solution of NaOH for 4 h. Then, the solution was filtered and centrifuged at 5000 rpm for 5 min. The melanin was precipitated from the solution using HCl at pH 2. This treatment was repeated twice to ensure a higher purity of melanin from other herbal metals. The melanin precipitate was thoroughly washed four times with high-purity distilled water, filtered, and dried overnight at 80°C.

For the synthesis of melanin doped with TiO_2 (TiO2-Mel), as shown in Fig. 1, 1g of melanin powder was dissolved in 20 mL of NaOH solution and mixed using ultrasonication for 5 min. One gram of TiO_2 powder was added to the melanin solution and stirred under UV light for seven hours. The color of the melanin solution gradually changed from black to gray and the production of oxygen gas increased due to the interaction between melanin and TiO_2. The resulting powder was dried in an air-drying oven at 80°C for one hour.

2.2 Characterization Techniques.

Fourier transmission infrared (FTIR) spectra for all samples were obtained using a Perkin-Elmer 580B IR spectrometer. Characteristic UV-Vis absorption spectra in the range between 200 to 800 nm were measured by a spectrophotometer (Perkin Elmer Lambda,40). Thermal gravimetry analysis (TGA) and differential scanning calorimetry (DSC) were performed on a TGA/DTA Mettler (Toledo, AG, Analytical CH-8603, Schwerzenbach, Switzerland) at a heating rate of 10°C/min under a flow of nitrogen. Transmission electron microscopy (TEM) images were obtained via FE-TEM (JEM-2100F JEOL, Japan) at an acceleration voltage of 80 kV.

3. Results And Discussion

3.1 Fourier transform infrared (FTIR) spectroscopic analysis

Figure 2 shows the FTIR transmission spectra of TiO_2, melanin and TiO_2-Mel in the range of 400–4000 cm^{-1}. The FTIR spectrum (A) of melanin shows a broad band at 3430.62 cm^{-1} due to the presence of the catechol (O-H) group, while the two bands at 2924.07 cm^{-1} and 2852.53 cm^{-1} are attributed to the C-H stretching vibration. The signals in the range of 3500 – 2800 cm^{-1} are associated with the stretching vibrations O-H and N-H in indole or pyrrole of the carboxylic acid and phenolic groups of melanin[27]. The band at 1650.58 cm^{-1} is attributed to aromatic C = C and/or carboxylate (COO-) groups[28]. The bands at 1545.41 cm^{-1} and 1411.90 cm^{-1} are attributed to the C-H groups[28]. The band at 1100.96 cm^{-1} is related to the asymmetric stretching of the C-N group.

In the TiO_2 spectrum (B), the broad band at 3428.58 cm^{-1} was due to stretching of the hydroxyl O–H bond, which represents the free surface adsorbed water molecules. Another band at 1633.38 cm^{-1} was

attributed to the bending vibration of water and Ti-OH[29]. The weak peaks at 2924.90 cm^{-1} and 1400.67 cm^{-1} can be assigned to the bending in functional groups CH [30]. The strong bands at approximately 447.76-682.84 cm^{-1} correspond to Ti-O stretching.

The spectrum (A) of TiO2-Mel is similar to that of melanin in the range of 4000 – 1700 cm^{-1}, but we noticed that it is more complicated nanostructure and has more functional groups. There was an increase in the intensity of some peaks in the range of 1700 ~ 1400 cm^{-1} corresponding to the bending vibration modes of the C = O double bond (COOH) and C = C and C-N bonds of the aromatic system and/or the carboxylate group (COO-). The intense peak at 1455.65 could be associated with COO – stretching vibrations in bridging and chelating bidentate Ti[31].

The C-N group shifted from 1100.96 cm^{-1} to 1169.11 cm^{-1}. The new peaks observed at 908.96 cm^{-1} and 866.90 cm^{-1} may be associated with the CH and CH_2 groups, respectively. A Ti-O stretching band was observed at 595.39 cm^{-1} after TiO_2 interacted with melanin molecules. This suggests that Ti was bound to oxygens in the functional groups of melanin (see Fig. 3).

3.2 Transmission Electron Microscopy (TEM)

Transmission electron microscopy (TEM) micrographs were employed to characterize and describe the shape and particle size of the nanoparticles of all samples, and the particle size distribution was measured using particle size analysis software(Image-J). As seen in the micrograph of the melanin sample in Fig. 2(A), melanin granules exhibited a spherical shape, which corresponds to the result previously reported in [32, 33]

In Fig. 2(B), TiO_2 appeared as aggregates with rod-like structures (approximately 12 nm×35 nm in size). This observation is consistent with that reported in the literature[33]. The TEM micrograph in Fig. 2(C) shows that the synthesized TiO2-Mel exists as an aggregate mix of ovoid and rod shapes with many different sizes, and TiO_2 nanoparticles were observed on the surface of melanin. The particle size distribution image shown in Fig. 2(D,E,F) correspond to mean diameters of 33.30 nm, 14.07 nm and 24.28 nm for melanin, TiO_2 and TiO2-Mel, respectively. This means that the hybrid (TiO2-Mel) became smaller in size compared to the melanin samples.

3.3 Thermal gravimetry analysis (TGA)

Figure 5 (A) Thermal gravimetry analysis (TGA) curves of TiO_2, melanin and TiO2-Mel samples. (B) The differential thermal analysis (DTA) curves of TiO_2, melanin and TiO2-Mel samples.

The TGA of TiO_2 nanoparticles shows no significant weight loss over the entire temperature range, which indicates that TiO_2 is thermally stable at high temperatures. Two main endothermic peaks of the DTA

curve of TiO_2 were observed. The first temperature of 63°C was attributed to the loss of absorbed water. The second temperature of 765°C was associated with the phase transformation from anatase TiO_2 to rutile TiO_2[34]. The TGA and DTA curves of melanin showed two clear steps of thermal degradation, beginning with a small weight loss of approximately 6.43% of its weight in the 65°C to 215°C range. The first endothermal peak appeared at 85°C, caused by the evaporation of bound water[32, 35]. An exothermal peak appeared immediately after that at 177°C, which was mainly due to the evolution of carbon dioxide[36]. Then, a continuous weight loss up to 66.47% was observed from 230°C to 500°C. An endothermal peak appeared at 273°C. This high percentage of weight loss could be explained by considering melanin degradation because of decarboxylation[36, 37]

The TGA curve of TiO2-Mel showed multiple steps of thermal degradation, with a large weight loss of approximately 13.43% of the sample weight in the 70°C to 120°C range. Then, there was a steady rate of weight loss of approximately 8.7% for each increase of 145°C, whereas the DTA curve confirms that the first endothermal peak that appeared at approximately 110°C was attributed to evaporation of water. We also observe here, as in the melanin curve, an exothermal peak immediately after the first endothermal peak at 150°C. Then, there were two endothermal peaks at 284°C and 470°C due to decarboxylation. After that, several similar endothermic peaks appear at 600°C, 758°C and 934°C. This may be associated with the possibility of titanium decomposition from the melanin molecule.

Table 1
Summary of the DTA endothermal peaks of TiO2-Mel

Assignment Peak	Inset	Offset	Peak
	T_i (°C)	T_f (°C)	T(°C)
1	70	138	110
2	246	388	284
3	415	515	470
4	524	667	600
5	693	834	758
6	855	999	934

3.4 Differential scanning calorimetry (DSC)

The differential scanning calorimetry of TiO_2, melanin, and TiO2-Mel samples are examined and the heat flow curves are shown in Fig. 6. Measurements were performed over the temperature range 25 to 500°C. Three characteristic endothermic peaks were observed for the TiO2-Mel at 44°C, 91°C and 115°C. These

endothermic peaks are associated with the evaporation of water. After the 150°C there is no reaction, which mean there are no crystallization and no melting happening.

The endothermic peak at 60°C for the TiO_2 sample is due to the decomposition of water molecules. A broad peak starts at 320°C ascribed to the transformation of

anatase TiO_2 nanoparticles to rutile. However, melanin DSC curve show four endothermic peaks, The first and larger peak at 100°C is corresponds to the moisture. The other three peaks appeared at 227°C, 299°C and 443°C respectively are mainly due to the decarboxylation as we explain in the TGA result.

3.5 Optical properties.

The optical absorption between 200 and 800 nm was investigated at room temperature. Figure 7 shows the optical absorption spectra of the TiO_2, melanin and melanin-doped TiO_2 (TiO2-Mel) nanoparticles with absorption peaks at 344, 233 and 213 nm, respectively, and the evaluation of their indirect bandgap. The observed absorption increases from 200 to 350 nm upon the incorporation of melanin molecules into the TiO_2 nanoparticles, and this absorption decreases exponentially and gradually in the visible light region in the TiO2-Mel sample, which indicates that the absorption in the ultraviolet region improved, as observed in Fig. 7, possibly due to the association of titanium metal with the -COOH functional groups in melanin. It can thus be concluded that the incorporation of melanin increased the shielding ability of TiO_2[38].

The band gap energy E_g was evaluated by the Tauc plot equation given by[39]

$$\alpha h\nu = K(h\nu - E_g)^n$$

where h is Planck's constant, A is a constant, ν is the incident radiation frequency, n is equal to ½ for an indirect band gap material and α is the absorption coefficient, which was calculated from the relation α= 2.303A/d, where d is the pathlength of light and A is the measured absorbance. The band gap energy E_g can be estimated by plotting $(\alpha h\nu)^{1/2}$ versus energy $h\nu$ and extrapolating the linear portion of the plot to the x-axis. The inset of Fig. 6 (A, B, C) shows that the band gap energies E_g of TiO_2, melanin and TiO2-Mel are 3.19 eV, 2.75 eV and 2.01 eV, respectively (Table 2).

It can be concluded that compared to TiO_2 and melanin, the energy band gap of TiO_2 doped with melanin (TiO_2-Mel) decreases. This behavior has been attributed to the induced energy rearrangement between TiO_2 and melanin due to the formation of C-O-Ti bonds[40]. Narrowing the band gap would improve the absorption of TiO_2-Mel in the visible light range. To understand more the enhanced the optical and thermal properties of melanin and titanium dioxide, Urbach energy have been calculated as seen in Fig. 8

and (listed in Table 2). Urbach energy describe the cavity exponential broadening of absorption edge which related to the thermal and disorder structural model of semiconductor either amorphas (as melanin) or crystalline (as titanium dioxide). According to this concept, the Urbach energy is determined by exponential of an empirical optical gap, which is defined according to the following relation known as Urbach rule[41]:

$$\alpha = \alpha_0 \exp\left(\frac{h\upsilon}{E_u}\right)$$

where α is the absorption coefficient, α_0 is characteristic parameter depend on material, hv is the incident photon energy and E_u is Urbach energy. It is observed that (TiO_2-Mel) Urbach energy enhancement comparing with samples of melanin and titanium dioxide, that means the formation of oxygen vacancies decreased after doped. The diminution of oxygen vacancy defects can be explained based on neutral charge concept. These oxygen vacancy defects decrease additional localised defect states which can effectively influence the edge of conduction and valance bands. This indicates an improvement in the structural properties and localized states of the hybrid (TiO_2-Mel).

Table 2
Experimental values for the absorption wavelength ,band gap ,Urbach energy variation of TiO_2, melanin and TiO_2-Mel.

Sample	Absorption wavelength λ (nm)	Bandgap (eV)	Urbach energy(eV)
TiO_2	344	3.19	0.241
Melanin	233	2.75	0.292
TiO_2-Mel.	213	2.01	0.102

4. Conclusion

The purpose of the current study was to synthesized a nanostructure hybrid of natural melanin/TiO_2 nanoparticles and characterized it by FTIR and SEM. In this paper our motivation was to explore the optical and thermal properties of this nanocomposite. The basic idea was to explore how the natural melanin would be affected by the TiO_2. It turned out that this research has raised many questions in need of further investigation in organic and inorganic polymers. However, natural melanin and TiO_2 played a

crucial role in preparing the melanin and TiO_2 composite systems. TiO_2 doped with melanin (TiO2-Mel) proved to be the important factor for improving the optical properties and enhancement in the nature of crystalline of hybrid (TiO2-Mel) depends on the Urbach energy results. One of the most spectacular results was the ability to had much higher absorption with a lower band gap than TiO_2. Another interesting feature was the thermal results, as we saw TGA and DSC provides a subtle means of understanding the thermal denaturation events when TiO2-Mel is heated. It showed that TiO2-Mel nanoparticles is thermally stable until 400°C, and at higher temperatures, titanium will decompose from the melanin molecule. Finally owing to the physical properties of Natural Melanin/ TiO_2 Nanostructure, this provides new routes for hybrid materials for new potential application such as organo-electronic devices, UV shielding and solar cell.

5. Declarations

Declaration of Interest Statement

The authors declare that they have no conflict of interest.

6. References

[1] Y. Yang, F. Wudl, Organic Electronics: From Materials to Devices, Adv. Mater. 21 (2009) 1401–1403. https://doi.org/10.1002/adma.200900844.

[2] Z.A. Lewicka, W.W. Yu, B.L. Oliva, E.Q. Contreras, V.L. Colvin, Photochemical behavior of nanoscale TiO2 and ZnO sunscreen ingredients, J. Photochem. Photobiol. A Chem. (2013). https://doi.org/10.1016/j.jphotochem.2013.04.019.

[3] S.M. Gupta, M. Tripathi, A review of TiO2 nanoparticles, Chinese Sci. Bull. (2011). https://doi.org/10.1007/s11434-011-4476-1.

[4] C. Luo, X. Ren, Z. Dai, Y. Zhang, X. Qi, C. Pan, Present Perspectives of Advanced Characterization Techniques in TiO2-Based Photocatalysts, ACS Appl. Mater. Interfaces. (2017). https://doi.org/10.1021/acsami.7b00496.

[5] B. O'Regan, M. Grätzel, A low-cost, high-efficiency solar cell based on dye-sensitized colloidal TiO2 films, Nature. (1991). https://doi.org/10.1038/353737a0.

[6] H. Wang, Y. Liu, M. Li, H. Huang, H.M. Xu, R.J. Hong, H. Shen, Multifunctional TiO2 nanowires-modified nanoparticles bilayer film for 3D dye-sensitized solar cells, Optoelectron. Adv. Mater. Rapid Commun. (2010).

[7] R. Srivastava, B.C. Yadav, Nanaostructured ZnO, ZnO-tio2 and ZnO-Nb2O5 as solid state humidity sensor, Adv. Mater. Lett. (2012). https://doi.org/10.5185/amlett.2012.4330.

[8] A. Rahimpour, M. Jahanshahi, B. Rajaeian, M. Rahimnejad, TiO2 entrapped nano-composite PVDF/SPES membranes: Preparation, characterization, antifouling and antibacterial properties, Desalination. (2011). https://doi.org/10.1016/j.desal.2011.05.049.

[9] H. Lin, A.K. Rumaiz, M. Schulz, D. Wang, R. Rock, C.P. Huang, S.I. Shah, Photocatalytic activity of pulsed laser deposited TiO2 thin films, Mater. Sci. Eng. B Solid-State Mater. Adv. Technol. (2008). https://doi.org/10.1016/j.mseb.2008.05.016.

[10] H. Tang, K. Prasad, R. Sanjinès, P.E. Schmid, F. Lévy, Electrical and optical properties of TiO2 anatase thin films, J. Appl. Phys. (1994). https://doi.org/10.1063/1.356306.

[11] A. Goossens, E.L. Maloney, J. Schoonman, Gas-Phase Synthesis of Nanostructured Anatase TiO2, Chem. Vap. Depos. (1998). https://doi.org/10.1002/(SICI)1521-3862(199805)04:03<109::AID-CVDE109>3.0.CO;2-U.

[12] S. Di Mo, W.Y. Ching, Electronic and optical properties of three phases of titanium dioxide: Rutile, anatase, and brookite, Phys. Rev. B. (1995). https://doi.org/10.1103/PhysRevB.51.13023.

[13] U. Bach, D. Lupo, P. Comte, J.E. Moser, F. Weissörtel, J. Salbeck, H. Spreitzer, M. Grätzel, Solid-state dye-sensitized mesoporous TiO2 solar cells with high photon-to-electron conversion efficiencies, Nature. (1998). https://doi.org/10.1038/26936.

[14] A. Wypych, I. Bobowska, M. Tracz, A. Opasinska, S. Kadlubowski, A. Krzywania-Kaliszewska, J. Grobelny, P. Wojciechowski, Dielectric Properties and Characterisation of Titanium Dioxide Obtained by Different Chemistry Methods, J. Nanomater. 2014 (2014) 124814. https://doi.org/10.1155/2014/124814.

[15] S.Y. Lee, S.J. Park, TiO2 photocatalyst for water treatment applications, J. Ind. Eng. Chem. (2013). https://doi.org/10.1016/j.jiec.2013.07.012.

[16] N.M. Dimitrijevic, S. Tepavcevic, Y. Liu, T. Rajh, S.C. Silver, D.M. Tiede, Nanostructured TiO2/polypyrrole for visible light photocatalysis, J. Phys. Chem. C. (2013). https://doi.org/10.1021/jp405562b.

[17] C. Sanchez, B. Julián, P. Belleville, M. Popall, Applications of hybrid organic-inorganic nanocomposites, J. Mater. Chem. (2005). https://doi.org/10.1039/b509097k.

[18] S.J. Blanksby, G.B. Ellison, Bond dissociation energies of organic molecules, Acc. Chem. Res. (2003). https://doi.org/10.1021/ar020230d.

[19] E. Filippo, C. Carlucci, A.L. Capodilupo, P. Perulli, F. Conciauro, G.A. Corrente, G. Gigli, G. Ciccarella, Enhanced photocatalytic activity of pure anatase Tio2 and Pt-Tio2 nanoparticles synthesized by green microwave assisted route, Mater. Res. (2015). https://doi.org/10.1590/1516-1439.301914.

[20] P. Meredith, T. Sarna, The physical and chemical properties of eumelanin., Pigment Cell Res. 19 (2006) 572–594. https://doi.org/10.1111/j.1600-0749.2006.00345.x.

[21] T.G. Costa, R. Younger, C. Poe, P.J. Farmer, B. Szpoganicz, Studies on synthetic and natural melanin and its affinity for Fe(III) ion, Bioinorg. Chem. Appl. 2012 (2012). https://doi.org/10.1155/2012/712840.

[22] V. Ball, D. Del Frari, M. Michel, M.J. Buehler, V. Toniazzo, M.K. Singh, J. Gracio, D. Ruch, Deposition Mechanism and Properties of Thin Polydopamine Films for High Added Value Applications in Surface Science at the Nanoscale, Bionanoscience. 2 (2012) 16–34. https://doi.org/10.1007/s12668-011-0032-3.

[23] P.P.A.P. Riley, Melanin, Int J Biochem Cell Biol. 29 (1997) 1235–1239. https://doi.org/10.1016/S1357-2725(97)00013-7.

[24] N. Madkhali, H.R. Alqahtani, S. Al, T. Amel, L. Adel, Control of optical absorption and fluorescence spectroscopies of natural melanin at different solution concentrations, Opt. Quantum Electron. (2019). https://doi.org/10.1007/s11082-019-1936-3.

[25] A. Laref, N. Madkhali, H.R. Alqahtani, X. Wu, S. Laref, Electronic structures and optical spectroscopies of 3d-transition metals-doped melanin for spintronic devices application, J. Magn. Magn. Mater. 491 (2019) 165513. https://doi.org/10.1016/j.jmmm.2019.165513.

[26] A.B. Mostert, B.J. Powell, F.L. Pratt, G.R. Hanson, T. Sarna, I.R. Gentle, P. Meredith, Role of semiconductivity and ion transport in the electrical conduction of melanin, Proc Natl Acad Sci U S A. 109 (2012) 8943–8947. https://doi.org/10.1073/pnas.1119948109.

[27] D.J. Kim, K.Y. Ju, J.K. Lee, The synthetic melanin nanoparticles having an excellent binding capacity of heavy metal ions, Bull. Korean Chem. Soc. 33 (2012) 3788–3792. https://doi.org/10.5012/bkcs.2012.33.11.3788.

[28] P. Vairale, V. Waman, A. Mayabadi, H. Pathan, S. Jadkar, V. Sathe, Electrochemical Synthesis of Melanin Thin Films: Evolution of Structural and Optical Properties, Int. J. Adv. Res. Phys. Sci. 1 (2014) 35–45. www.arcjournals.org.

[29] T.S. R., P. A.P.S., R. Niranjan, M. Kaushik, T. Devasena, J. Kumar, R. Chelliah, D.H. Oh, S. Swaminathan, D.V. G., Metal oxide curcumin incorporated polymer patches for wound healing, Appl. Surf. Sci. (2018). https://doi.org/10.1016/j.apsusc.2018.01.143.

[30] A. León, P. Reuquen, C. Garín, R. Segura, P. Vargas, P. Zapata, P.A. Orihuela, FTIR and raman characterization of TiO2 nanoparticles coated with polyethylene glycol as carrier for 2-methoxyestradiol, Appl. Sci. (2017). https://doi.org/10.3390/app7010049.

[31] A. Pezzella, L. Capelli, A. Costantini, G. Luciani, F. Tescione, B. Silvestri, G. Vitiello, F. Branda, Towards the development of a novel bioinspired functional material: Synthesis and characterization of hybrid TiO 2/DHICA-melanin nanoparticles, Mater. Sci. Eng. C. (2013). https://doi.org/10.1016/j.msec.2012.08.049.

[32] L.F. Wang, J.W. Rhim, Isolation and characterization of melanin from black garlic and sepia ink, LWT. (2019). https://doi.org/10.1016/j.lwt.2018.09.033.

[33] N. Madkhali, H.R. Alqahtani, S. Al-Terary, A. Laref, A. Haseeb, The doping effect of Fe, Cu and Zn ions on the structural and electrochemical properties and the thermostability of natural melanin extracted from Nigella sativa L, J. Mol. Liq. (2019). https://doi.org/10.1016/j.molliq.2019.04.063.

[34] M.M. Mahlambi, A.K. Mishra, S.B. Mishra, R.W. Krause, B.B. Mamba, A.M. Raichur, Comparison of rhodamine B degradation under UV irradiation by two phases of titania nano-photocatalyst, in: J. Therm. Anal. Calorim., 2012. https://doi.org/10.1007/s10973-011-1852-7.

[35] A.M. Gómez-Marín, C.I. Sánchez, Thermal and mass spectroscopic characterization of a sulphur-containing bacterial melanin from Bacillus subtilis, J. Non. Cryst. Solids. (2010). https://doi.org/10.1016/j.jnoncrysol.2010.05.054.

[36] I.E. Pralea, R.C. Moldovan, A.M. Petrache, M. Ilieș, S.C. Hegheș, I. Ielciu, R. Nicoară, M. Moldovan, M. Ene, M. Radu, A. Uifălean, C.A. Iuga, From extraction to advanced analytical methods: The challenges of melanin analysis, Int. J. Mol. Sci. (2019). https://doi.org/10.3390/ijms20163943.

[37] S.S. Sajjan, O. Anjaneya, G.B. Kulkarni, A.S. Nayak, S.B. Mashetty, T.B. Karegoudar, Properties and functions of melanin pigment from Klebsiella sp. GSK, Korean J. Microbiol. Biotechnol. (2013). https://doi.org/10.4014/kjmb.1210.10002.

[38] W. Xie, E. Pakdel, D. Liu, L. Sun, X. Wang, Waste-Hair-Derived Natural Melanin/TiO2 Hybrids as Highly Efficient and Stable UV-Shielding Fillers for Polyurethane Films, ACS Sustain. Chem. Eng. (2020). https://doi.org/10.1021/acssuschemeng.9b03514.

[39] Shimadzu Corporation, Measurements of Band Gap in Compound Semiconductors - Band Gap Determination from Diffuse Reflectance Spectra -, Measurement. (1800).

[40] W. Xie, E. Pakdel, Y. Liang, D. Liu, L. Sun, X. Wang, Natural melanin/TiO2 hybrids for simultaneous removal of dyes and heavy metal ions under visible light, J. Photochem. Photobiol. A Chem. (2020). https://doi.org/10.1016/j.jphotochem.2019.112292.

[41] F. Urbach, The Long-Wavelength Edge of Photographic Sensitivity and of the Electronic Absorption of Solids, Phys. Rev. 92 (1953) 1324. https://doi.org/10.1103/PhysRev.92.1324.

Figures

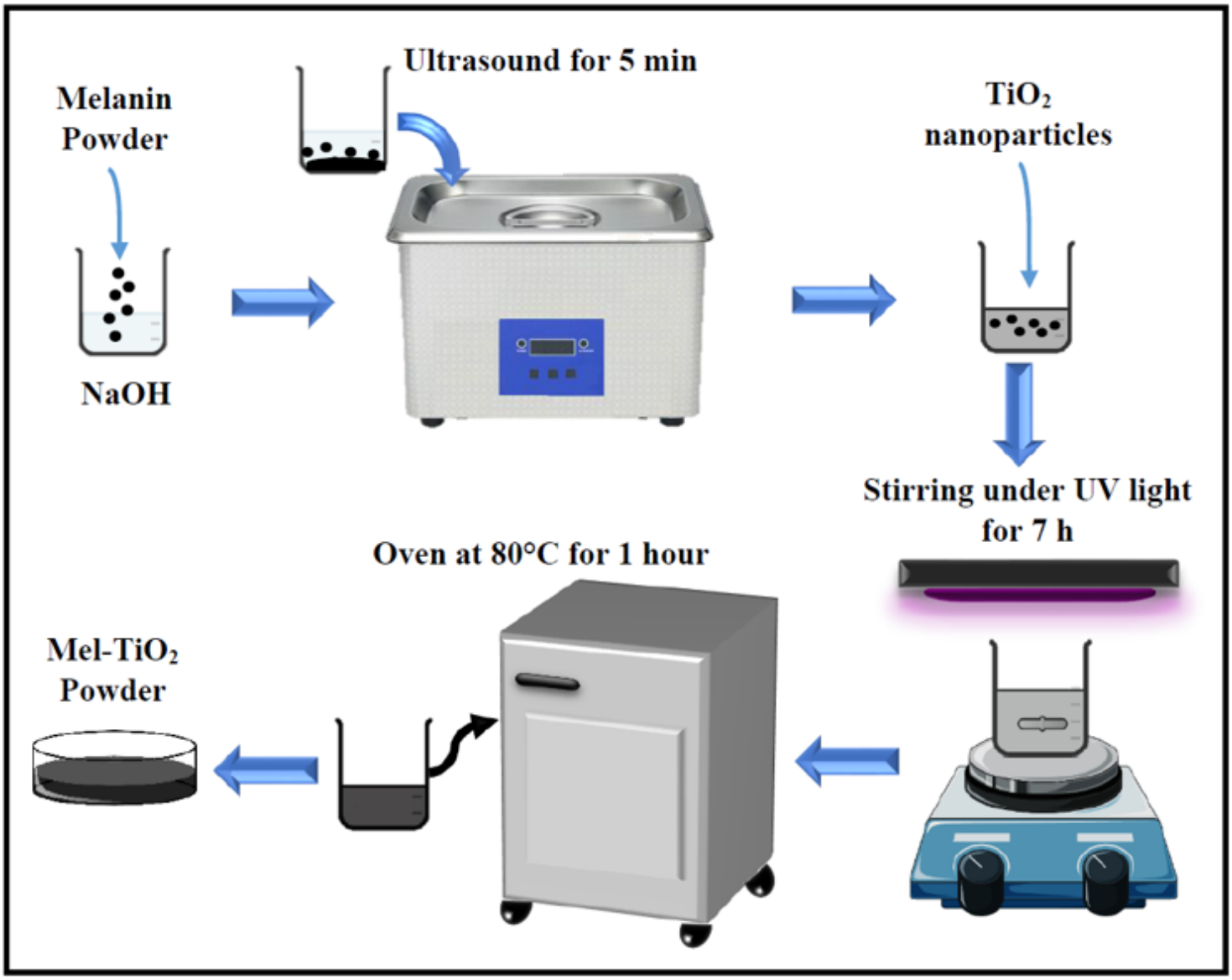

Figure 1

Schematic of the process followed for the synthesis of TiO2-Mel

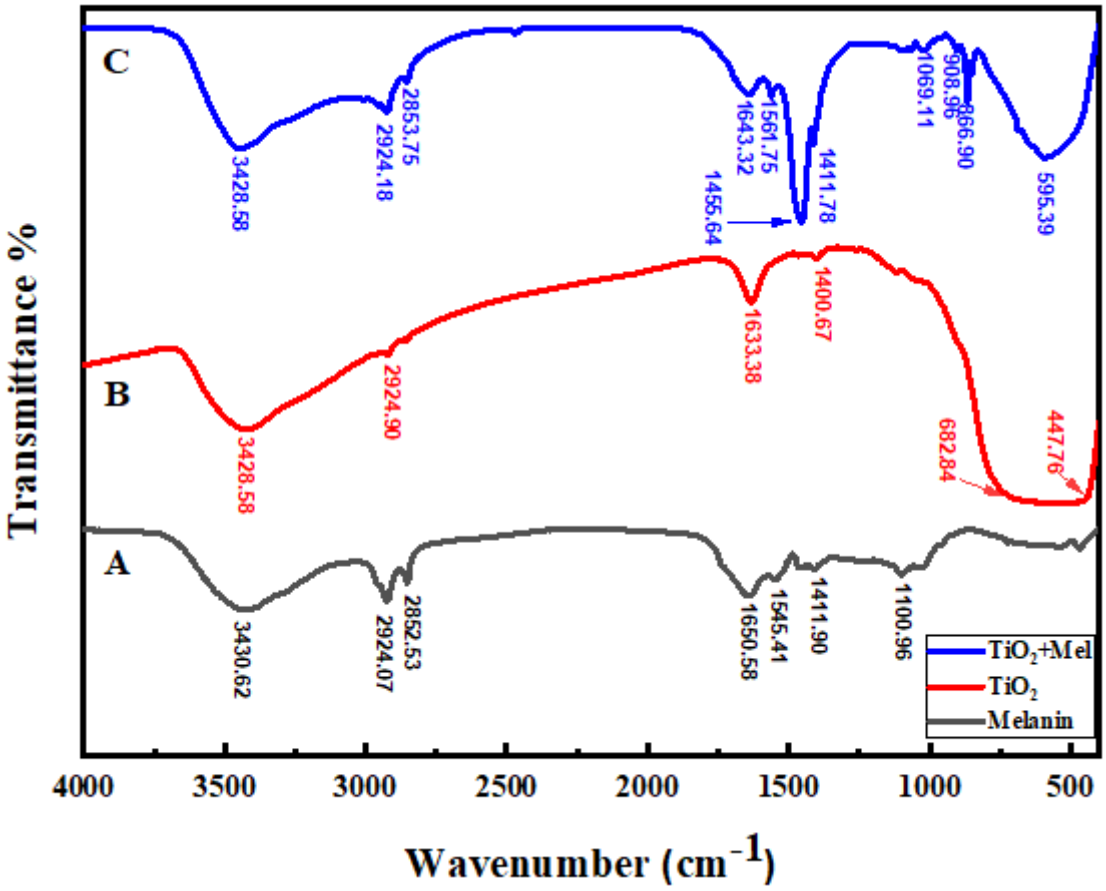

Figure 2

FTIR spectra of TiO2, melanin and TiO2-Mel samples.

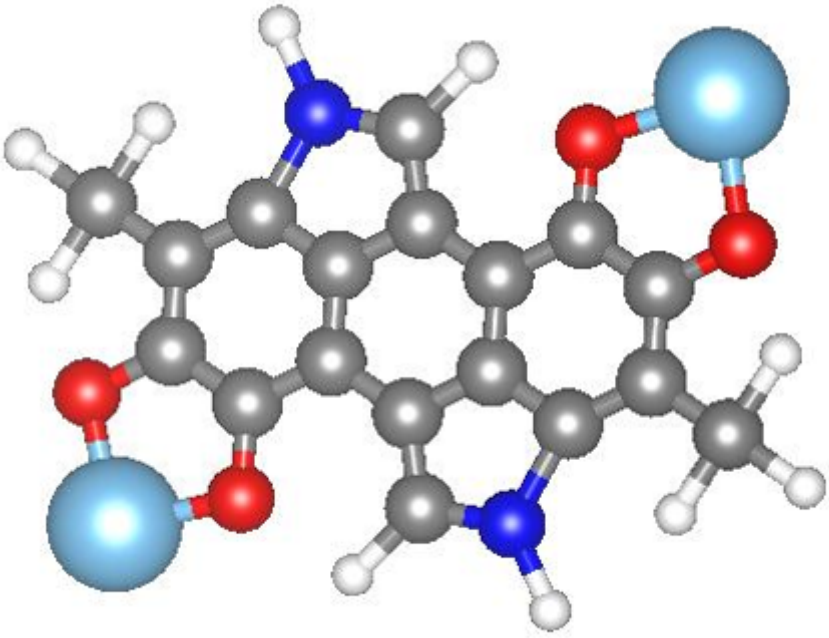

Figure 3

Scheme of the molecular structure of TiO2-Mel. (gray: C, red: O, blue: N, white: H, aqua: Ti).

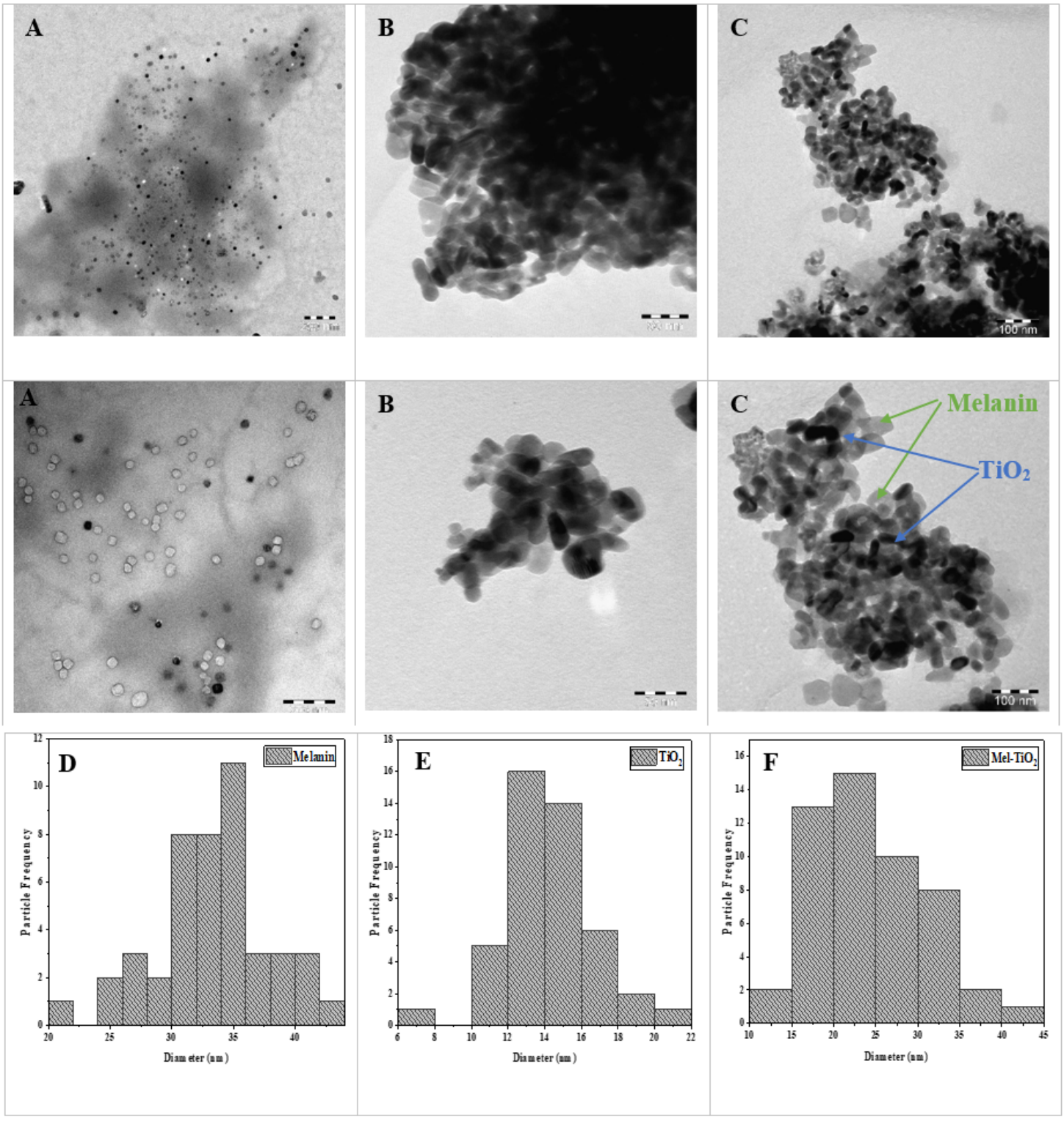

Figure 4

(A) TEM images of melanin, (B) TEM images of TiO2, (C) TEM images of TiO2-Mel, (D) particle size distribution of melanin, (E) particle size distribution of TiO2, (F) particle size distribution of TiO2-Mel

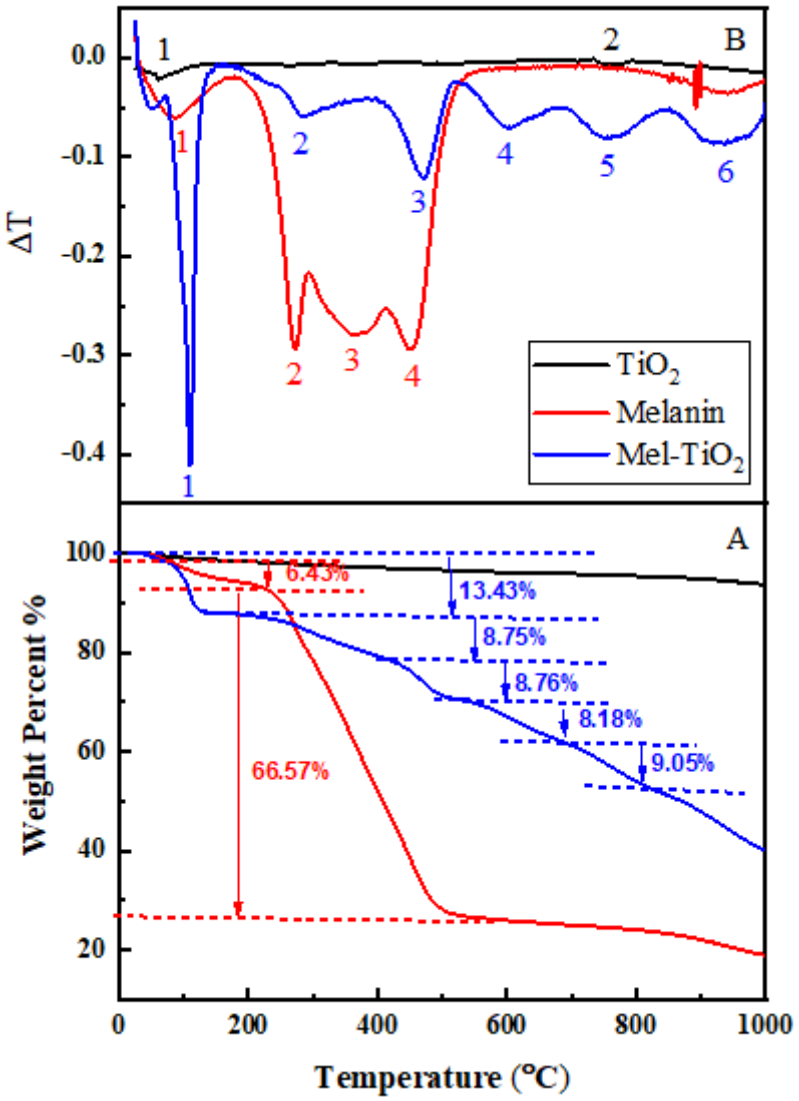

Figure 5

(A) Thermal gravimetry analysis (TGA) curves of TiO2, melanin and TiO2-Mel samples. (B) The differential thermal analysis (DTA) curves of TiO2, melanin and TiO2-Mel samples.

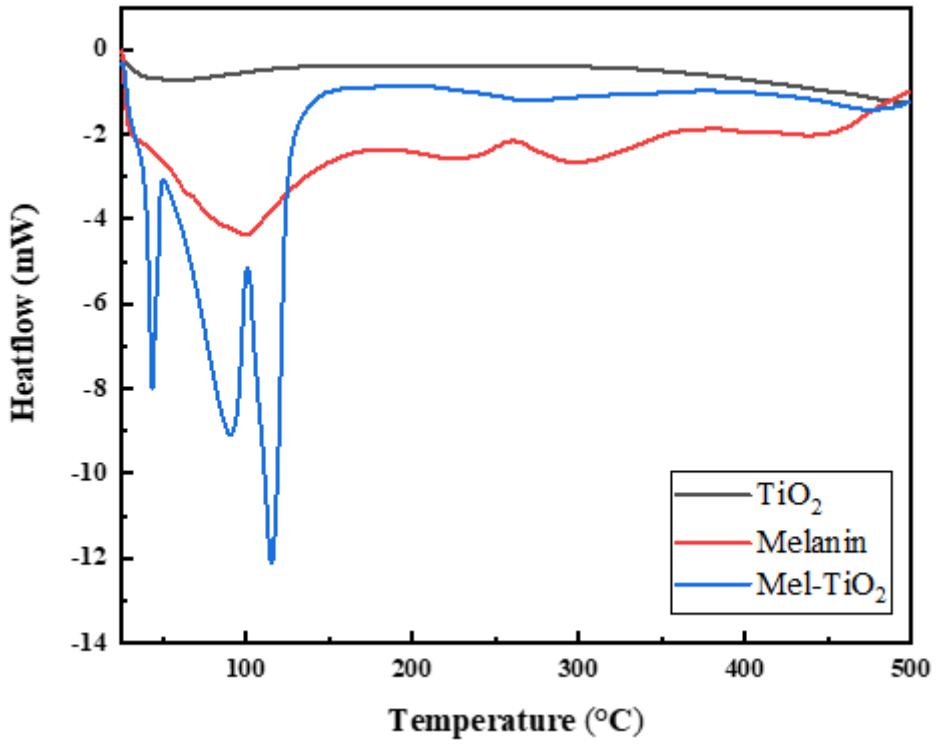

Figure 6

Differential scanning calorimetry (DSC) curves of TiO2, melanin and TiO2-Mel samples.

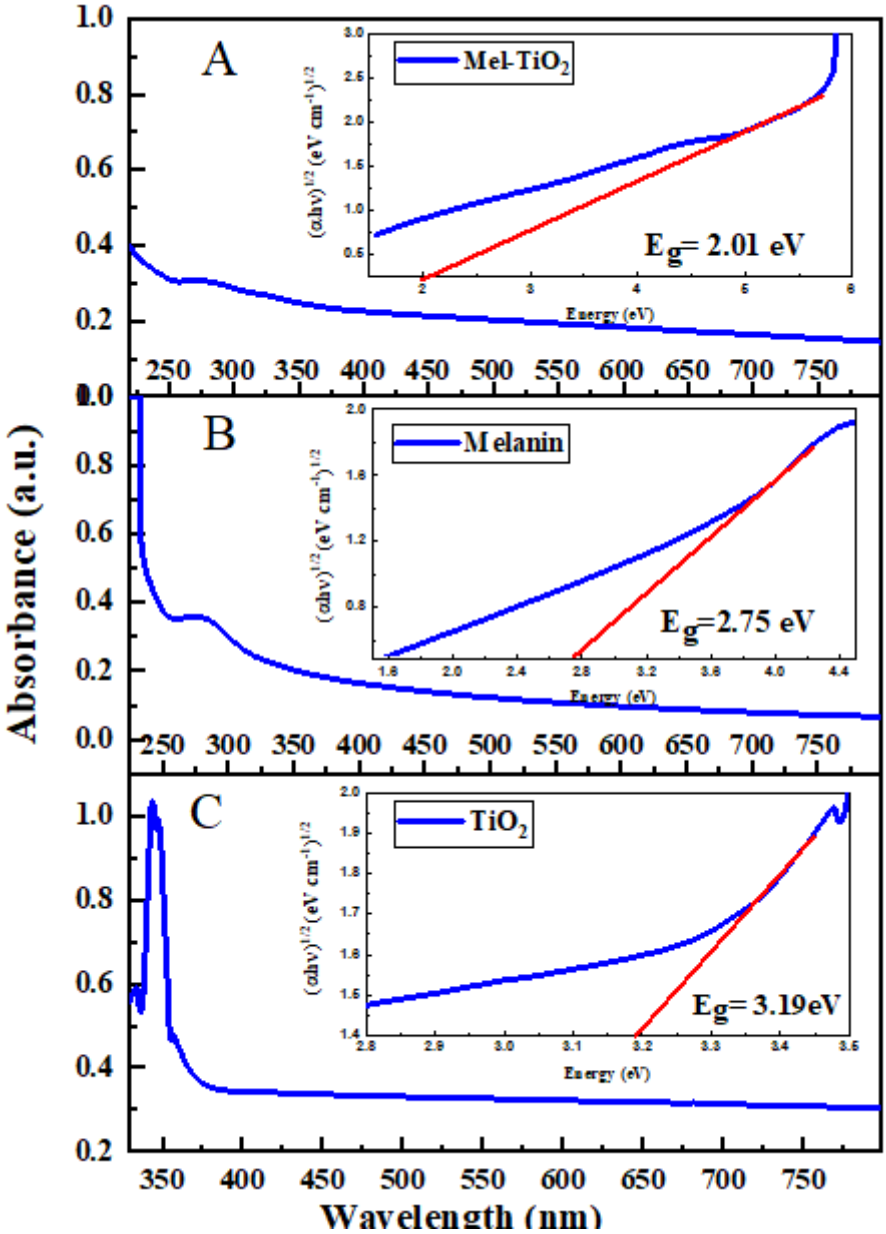

Figure 7

(A) The optical absorbance spectrum of TiO2-Mel; the inset shows the corresponding bandgap energy calculated by Tauc plots. (B) The optical absorbance spectrum of melanin; the inset shows the corresponding bandgap energy calculated by Tauc plots. (C) The optical absorbance spectrum of TiO2; the inset shows the corresponding bandgap energy calculated by Tauc plots.

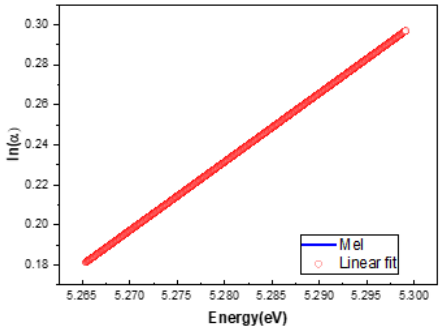

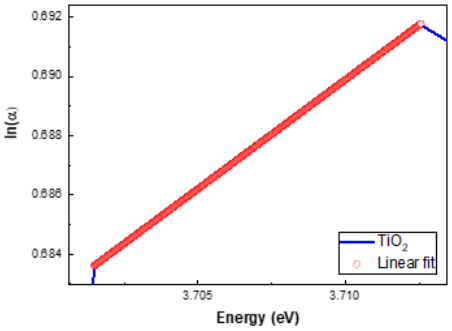

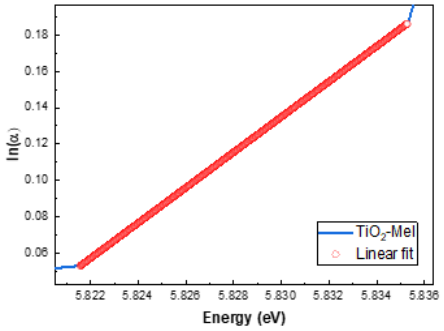

Figure 8

Determination of Urbach energy for (Mel,TiO2 and TiO2-Mel)